Raman and infrared phonon piezospectroscopy in InP

E. Anastassakis and Y. S. Raptis
Physics Department, Laboratory III, National Technical University, Zografou Campus, Athens 15773, Greece

M. Hünermann and W. Richter
I. Physikalisches Institut der Rheinisch-Westfälischen Technischen Hochschule Aachen, D-5100 Aachen, Federal Republic of Germany

M. Cardona
Max-Planck-Institut für Festkörperforschung, Heisenbergstrasse 1, D-7000 Stuttgart 80, Federal Republic of Germany

(Received 28 March 1988)

We have studied the effect of a uniaxial stress on the long-wavelength optical phonons of InP using Raman and far-infrared spectroscopic techniques. The Raman measurements were performed with laser lines in regions of both transparency and opacity, using infrared and visible lasers, respectively. Phonon and effective-charge deformation potentials have been obtained from the data, and also an estimate of the Faust-Henry coefficient from the integrated scattering intensities. Comparison of the Raman and infrared reflectivity results allows us to conclude that the applied stress is relaxed toward the surface of the sample.

I. INTRODUCTION

The dependence of the long-wavelength optical-phonon frequencies on uniaxial stress X has received considerable attention in recent years, in connection with the characterization of lattice-mismatched (strained) superlattices and heterostructures.[1] Of central importance in these studies is the knowledge of the so-called phonon deformation potentials (PDP's) which describe strain-induced frequency shifts of phonons. The PDP's are components of a fourth-rank tensor K_{ij}^{σ}, in suppressed index notation, where σ identifies the long-wavelength optical phonon under consideration, at frequency $\omega_{\sigma}{}^{2}$. Quantitatively K_{ij}^{σ} stands for the derivative of the ith component of the effective force constant of the phonon σ, relative to the jth component of strain. K_{ij}^{σ} can be calculated from the slopes $\Delta\Omega/X$ of the phonon frequency shifts $\Delta\Omega$ versus X, as derived from certain piezospectroscopy experiments with appropriately chosen configurations. There are three types of such experiments: (i) conventional Raman scattering with visible lasers (VISRS),[3] (ii) Fourier transform far-infrared (FIR) reflectivity,[4,5] and most recently, (iii) Raman scattering with infrared lasers (IRRS).[6-8] The criterion for preferring VISRS or IRRS is to have scattering from the bulk of the material, i.e., to use a laser in the region of transparency. In this way the PDP's obtained are more representative of the bulk where the elastic strain is more accurately known. Also, if the sample is transparent forward scattering experiments can be performed, leading to information not available in backscattering.[6] Thus, VISRS can and has been used for insulators (e.g., diamond,[9] fluorites[10,11]) and for large-gap semiconductors [e.g., zinc-blende-type semiconductors ZnSe, (Ref. 12) and GaP (Ref. 13)]. IRRS, on the other hand, is particularly appropriate for small-gap semiconductors. There exists one type of ir laser commercially available and suitable for Raman spectroscopy, i.e., the cw Nd:YAG (yttrium aluminum garnet) laser, operating at $\omega_L = 1.165$ eV or 9396.7 cm^{-1} ($\lambda_L = 1.0642$ μm). This laser is appropriate for a limited class of semiconductors with energy gaps ω_g larger than ω_L and still smaller than visible frequencies (1.55–2.8 eV). GaAs ($\omega_g = 1.43$ eV) and AlSb ($\omega_g = 1.61$ eV) are the only such materials for which PDP values have been obtained with a Nd:YAG laser (Refs. 6, 7, and 8, respectively).

In all other cases reported so far, VISRS has been used in either 180° and 90° scattering geometries with transparent materials or only 180° geometry with opaque materials. In the latter case, the scattering volume is limited by the penetration depth near the surface where relaxation of the applied uniaxial stresses may occur. The PDP values obtained in this way are necessarily affected by such stress relaxations. An additional disadvantage in this case (of 180° geometry with opaque materials) is that, contrary to IRRS, not all components K_{ij}^{σ} can be determined, due to the stringent selection rules imposed by this geometry.

Finally, the FIR reflectivity experiments involve measurements in the reststrahlen region which is characterized by large variations of the penetration depth with frequency. The average interaction volume in this case extends deeper into the material than in the case of VISRS. Accordingly, the corresponding PDP values are expected to be affected by stress relaxation to a lesser degree than in VISRS. In addition, reflectivity measurements offer the following advantages. Firstly, they allow estimates of all components of $\mathbf{K}^{\sigma}$. Secondly, it is much easier than in Raman scattering to study the free-carrier characteristics under uniaxial stress applied to doped materials.[5] Also,

to the extent that the penetration depths in the reststrahlen region can be altered by doping, it might be possible to probe the stress relaxation at variable average depths.

Indium phosphide is a III-V zinc-blende-type semiconductor with a wide range of applications in optoelectronics[14] and band-gap engineering.[15] Values for its PDP's do not seem to have been measured although the need for such values has already been expressed.[16] Its direct gap, $E_g = 1.35$ eV at 300 K,[17] renders InP transparent to the Nd:YAG laser radiation. Thus, all three types of experiments can be performed on InP, that is, IRRS, FIR reflectivity, and VISRS. It is the purpose of this work to report on the results of such experiments. The main objectives are to establish accurate values for the PDP's of InP, obtain an estimate for its Faust-Henry coefficient,[18] and attempt to correlate the differences in the results of the three experiments on the basis of a stress relaxation model. To simplify notation and units, we use throughout this work the dimensionless PDP's defined by $\tilde{K}_{ij}^{\sigma} = K_{ij}^{\sigma}/\omega_{\sigma}^2$ (Ref. 2) where σ stands either for T (transverse-optical phonons, TO) or for L (longitudinal-optical phonons, LO).[19]

II. EXPERIMENTAL DETAILS

The samples were cut from single-crystal nominally undoped InP ingots in the form of parallelepipeds ($1.5\times1.5\times15$ mm^3). For the IRRS measurements the samples were glued into brass cups[6] while for the FIR and VISRS measurements they were held by friction between polished pistons covered with small pieces of fused silica.[5] Different stress machines were used for the three experiments, all calibrated against standard weights to within 0.03 GPa.

Four different crystal orientations were used, defined by

$$(x,y,z)=([100],[010],[001]) \text{ or } \mathbf{a} , \tag{1a}$$

$$(x',y',z')=([1\bar{1}0],[110],[001)] \text{ or } \mathbf{b} , \tag{1b}$$

$$(x'',y'',z'')=([11\bar{2}],[\bar{1}10],[111]) \text{ or } \mathbf{c} , \tag{1c}$$

$$(x''',y''',z''')=([110],[001],[1\bar{1}0]) \text{ or } \mathbf{d} . \tag{1d}$$

The stress X was always applied along the vertical (V) direction z, z', z'', and z''', the horizontal (H) plane being always defined by the other two axes. All measurements were taken at room temperature. For the IRRS measurements the experimental setup included, besides the cw Nd:YAG laser, a liquid-N_2-cooled Ge detector and a Jarrel-Ash double monochromator. The detector signal was fed through a lock-in amplifier and an analog-to-digital converter into an HP-9216 computer for data analysis. The spectral resolution was 2.7 cm^{-1}. More details about these measurements can be found in Ref. 6.

The FIR reflectivity experiments were carried out in the spectral range $\omega = 100$–350 cm^{-1} using a modified Bruker rapid scan Fourier spectrometer with a spectral resolution of 0.13 cm^{-1}. The reflectivity of the sample under stress was determined from[5]

$$R(\omega,X)=R(\omega,0)I(\omega,X)/I(\omega,0) , \tag{2}$$

where $R(\omega,0)$ is the zero stress reflectivity of the sample measured against a standard mirror before mounting the sample on the stress machine. $I(\omega,0)$ and $I(\omega,X)$ are the intensities reflected by the sample mounted in the stress machine under zero stress or under stress X. This procedure eliminates all parameters of the stress apparatus and the spectrometer affecting the intensities of the reflected light beams except those influenced by the sample reflectivity. More details can be found in Ref. 5.

The VISRS measurements were taken with a Spex double monochromator (spectral resolution 3 cm^{-1}), an RCA-31034-cooled photomultiplier, and a photon counting detection system. The 476.5-nm line of an Ar^+ laser was used at low powers ($\lesssim 150$ mW) focused onto the sample with a cylindrical lens to avoid heating. The frequency scale was calibrated against a Ne lamp and analyzed on a LeCroy 3500 MCA. More details about the experimental procedure can be found in Ref. 11.

III. EXPERIMENTAL RESULTS

A. ir Raman scattering experiments

All faces of the samples (n type) were polished with Syton (Monsanto Corp. St. Louis, MO). All four crystal orientations **a**–**d** were used in these experiments, with the scattered light always being detected along x, x', x'', and x''', respectively. Orientation **d**, in particular, was used for consistency checks.[6] In configurations **a**–**c**, both TO and LO phonons vibrate at different frequencies when polarized parallel to the stress (singlet components at frequencies ω_{Ts} and ω_{Ls}) or perpendicular to the stress (doublet components ω_{Td} and ω_{Ld}). In configuration **d**, the doublets, in addition, break into two singlets each. Various scattering geometries for observing each of these components have been used in Refs. 6–8, and tabulated in detail in Ref. 8. The ω_{Ls} component, in particular, can only be observed in the so-called oblique forward geometry, with a vertical scattering plane and an external angle of incidence $\theta_V \sim 20°$ (scattering wave vector along the stress axis).

Figure 1 shows all components of interest for $X=0$ and $X\neq 0$ taken with various geometries in the **b** orientation. All ω_T and ω_L frequencies observed in these and other spectra were calibrated, respectively, against the line of a Hg lamp (9099.3 cm^{-1}, third-order spectrum) and an Ar lamp (9023.7 cm^{-1}, first-order spectrum, not shown in Fig. 1).

Figures 2 and 3 display the frequency shifts of the eight phonon components measured with $\mathbf{X}\|[001]$ and $\mathbf{X}\|[111]$, respectively, in various scattering geometries. Figure 2 also includes typical data for $\mathbf{X}\|[1\bar{1}0]$. The geometries used for each component are listed in Table I together with the coefficients of a linear (a) and a quadratic (A,B) least-squares fit as well as the zero stress frequency $\omega_{T,L}$ obtained from such fits. Since the nonlinearities shown in Figs. 2 and 3 were systematic and not negligible, we decided to base all subsequent calculations on the slope A and the average zero stress values $\omega_{T,L}$ obtained from the quadratic fit. These frequencies are $\omega_T = 303.7$ cm^{-1} and $\omega_L = 350.6$ cm^{-1}. Whereas ω_T is

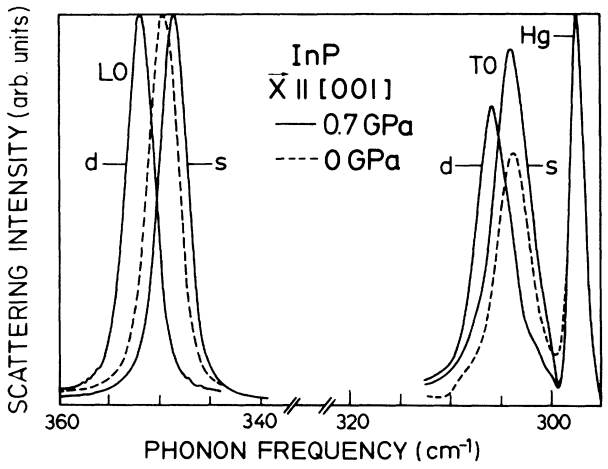

FIG. 1. Infrared Raman spectra (**b** orientation, see text) of the singlet (*s*) and doublet (*d*) components of TO and LO phonons of InP at 300 K. Dashed line: $X=0$, oblique forward geometry, vertical (horizontal) and horizontal (horizontal) polarizer for the incident (scattered) light, for the TO and LO phonons, respectively. *d*,*s* components: $X=0.7$ GPa along [001]. TO*d*, TO*s*, backward geometry, vertical (horizontal), and horizontal (horizontal) polarizations, respectively. LO*d*, LO*s*, 90°, and oblique forward geometry, respectively, polarizations as for TO*d*, TO*s*, respectively. The vertical scale is different for each spectrum. The laser power on the sample was 1.2 W. The Hg line at 297.43 cm^{-1} was used for calibration of the TO frequencies. An Ar line at 373 cm^{-1} (not shown) was used for calibration of the LO frequencies.

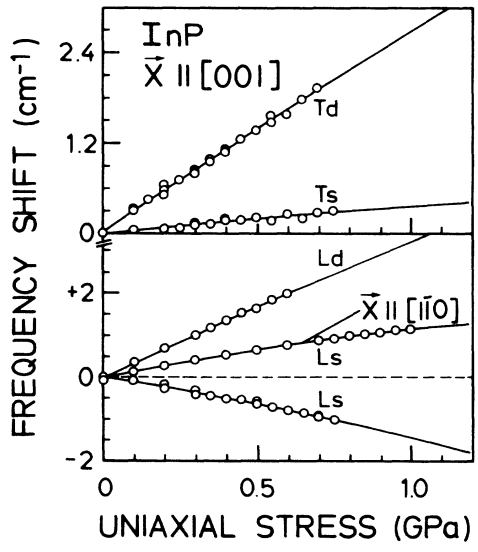

FIG. 2. IRRS frequency shifts vs compressive stress for the four phonon components of InP (*Td*,*s*; *Ld*,*s*) with **X**||[001], and for one out of six components (*Ls*) with **X**||[1$\bar{1}$0]. The corresponding scattering geometries are listed in Table I. The solid lines represent quadratic least-squares fits to the combined data (Table I). The dashed line is parallel to the axis. In determining the slopes, the compressive stress is taken as negative.

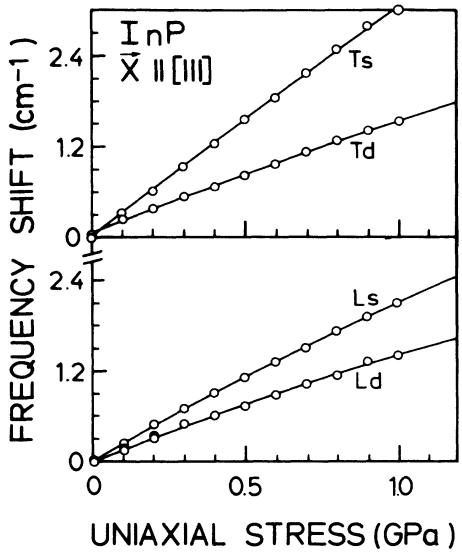

FIG. 3. Same as Fig. 2 for **X**||[111].

very close to the values from other Raman studies reported in the literature (e.g., 303.3 cm^{-1}, Ref. 20), the value of ω_L observed here is systematically higher by ~ 6 cm^{-1} (344.5 cm^{-1}, Ref. 20). We believe this is the result of free carriers coupling to the LO phonon. The carrier concentration necessary to produce a shift of 6 cm^{-1} is calculated to be 1.3×10^{17} cm^{-3}. During all measurements leading to the data of Figs. 2 and 3 care was taken to avoid mixing of forward (θ_V) and backward (180°) scattering which may arise from the reflected part of the incident beams inside the crystal.[6] The maximum stress values reached in these experiments were ≤ 0.75 GPa (1.0 GPa) corresponding to orientations **a**,**b** (**c**,**d**). No signs of irreversible plastic deformations were observed, contrary to the case of GaAs.[6] The $X=0$ frequencies were recovered each time after releasing the stress. It is noted that for **X**||[001] ([111]) the *d* (*s*) components shift faster than the *s*(*d*) components, a behavior similar to that of all tetrahedral semiconductors (but not to that of diamond[9]). Furthermore, the *Ls* component for **X**||[001] exhibits softening with compressive stress, similar to observations in GaP (Ref. 13) and AlSb.[8]

Table II includes the values of the mode Grüneisen parameters γ_σ and the differences $\tilde{K}^{\sigma}_{11}-\tilde{K}^{\sigma}_{12}$ which are calculated from known expressions (Table I in Ref. 8). From these and the relationship $\tilde{K}^{\sigma}_{11}+2\tilde{K}^{\sigma}_{12}=3\gamma_\sigma$ we obtain the values of PDP's shown in Table II. The values of γ_σ found here are very close to those obtained from hydrostatic pressure work[20] but are larger than those from the FIR and VISRS data.

As a consistency check of the slopes obtained with orientations **a**, **b**, and **c**, we compare the experimental slope for the singlet of the longitudinal phonon listed under orientation **d** (Table I, -1.54 ± 0.05) with the value calculated from the data of orientations **a**, **b**, and **c**. A straightforward calculation shows that

$$\Delta\omega^{d}_{Ls}=\Delta\omega^{H}_{L}+\tfrac{1}{6}\Delta\omega^{a}_{L}+\tfrac{1}{2}\Delta\omega^{c}_{L}\ . \qquad (3)$$

TABLE I. Stress orientation, scattering configuration, light polarizations, and slope coefficients A,B (a) obtained from quadratic (linear) fits to the data, for the various stress-split phonon components of InP at room temperature. The data from the ir Raman scattering measurements were used. The uncertainty in ω_σ, A, B, a is ± 0.05, in the corresponding units, and is due to the scatter of the experimental points for various repeated measurements. θ_V indicates oblique forward scattering in a vertical plane. V (H) means vertical (horizontal) polarization for the incident (scattered) light in the infrared Raman scattering experiments. $\perp$ ($\parallel$) means light polarized $\perp X$ ($\parallel X$) in the infrared reflectivity experiments. The average uncertainty for the slope a (linear fit only) is ± 0.1.

Crystal orientation	Configuration		Method	Phonon component	Quadratic fit ω_σ (cm^{-1})	Quadratic fit A (cm^{-1}/GPa)	Quadratic fit B (cm^{-1}/GPa^2)	Linear fit ω_σ (cm^{-1})	Linear fit a (cm^{-1}/GPa)
c	180°	*VH*	IRRS	*Td*	303.8	−1.63	−0.14	303.8	−1.49
X$\parallel$[111]		$\perp$	FIR						−1.00
	180°	*VV*	IRRS	*Ts*	303.7	−3.17	−0.13	303.7	−3.05
		$\parallel$	FIR						−2.28
	90°	*HH*	IRRS	*Ld*	350.4	−1.62	−0.22	350.4	−1.42
		$\perp$	FIR						−1.32
	θ_V	*VV*	IRRS	*Ls*	350.4	−2.32	−0.25	350.4	−2.09
		$\parallel$	FIR						−1.97
b,**a**	180°(**b**)								
X$\parallel$[001]	90°(**a**)	*VH*	IRRS	*Td*	303.8	−2.79	−0.14	303.8	−2.71
	θ_V(**b**)	$\perp$	FIR						−1.78
	180°(**b**)	*HH*	IRRS	*Ts*	303.6	−0.45	−0.08	303.6	−0.40
	90°(**a**)	$\parallel$	FIR						−0.31
	90°(**a**)	*VH*	IRRS	*Ld*	350.7	−3.55	−0.32	350.7	−3.37
		$\perp$	FIR						−2.23
	θ_V(**b**)	*HH*	IRRS	*Ls*	351.2	+1.16	−0.30	351.2	+1.37
		$\parallel$	FIR						+1.23
d	θ_V	*VH*	IRRS	*Ls*	350.3	−1.54	−0.37	350.4	−1.18
X$\parallel[1\bar{1}0]$									

When referred to unit compressive stress, $\Delta\omega_{Ls}^d$ is the slope of the *Ls* component in orientation d, $\Delta\omega_L^H$ is the slope of the hydrostatic shift of the LO phonon measured in either **a** or **b** or **c**, $\Delta\omega_L^a$ is the splitting in **a** or **b** (i.e., slope of *Ls* minus slope of *Ld*), and $\Delta\omega_L^c$ is the splitting in **c**. With $\Delta\omega_L^H = -1.92$ (average of **a** and **c** values), $\Delta\omega_L^a = 4.71$, and $\Delta\omega_L^c = -0.70$ we find from Eq. (3) $\Delta\omega_{Ls}^d = -1.5 \pm 0.1$, which compares very favorably with the experimental value of -1.54 ± 0.05.

TABLE II. Mode Grüneisen parameters and phonon deformation potentials for the transverse and the longitudinal (in parentheses) long-wavelength optical phonons based on ir Raman scattering and FIR reflectivity data.

$\gamma_{T(L)}$	1.48(1.19)±0.04	IRRS
	0.96(0.82)±0.05	FIR
	1.44(1.24)±0.02	Ref. 20
$\tilde{K}_{11}^{T(L)} - \tilde{K}_{12}^{T(L)}$	0.69(1.20)±0.02	IRRS
	0.42(0.90)±0.04	FIR
$\tilde{K}_{11}^{T(L)}$	−2.5(−1.6)±0.1	IRRS
	−1.6(−1.0)±0.1	FIR
$\tilde{K}_{12}^{T(L)}$	−3.2(−2.8)±0.1	IRRS
	−2.1(−1.9)±0.1	FIR
$\tilde{K}_{44}^{T(L)}$	−0.47(−0.18)±0.02	IRRS
	−0.38(−0.18)±0.04	FIR

Once the PDP's are known, a number of relevant microscopic parameters can be calculated such as the effective charge deformation parameters $\tilde{M}_{ij}$.[6,21] The values k_{ij}^e of the high-frequency photoelastic constants which are needed for such calculations are taken from Refs. 22–24 and are listed in Table III together with the static (low-frequency) values k_{ij}^0 of the photoelastic constants. The latter are easily derived from the PDP's and k_{ij}^e (Ref. 21). The resulting values of $\tilde{M}_{ij} = (\partial \ln e_T^*/\partial\epsilon)_{ij}$ are included in Table III together with the volume and pressure coefficients $\gamma^* = -(\partial \ln e_T^*/\partial \ln V)$ and $\partial e_T^*/\partial P$ of the effective charge, and the volume coefficient $\partial \ln \epsilon_\infty/\partial \ln V$ of the optical dielectric constant. In Table III we have also listed theoretical values for the same parameters obtained from a semiempirical bond-orbital theory of the effect of strain on the effective charge.[25,26]

A final parameter calculated from these measurements is the Faust-Henry coefficient C (Ref. 18). It is given by[27]

$$C=\left[\frac{\omega_L^2-\omega_T^2}{\omega_T^2}\right]\left\{1\pm\left[\left[\frac{\bar{n}_T+1}{\bar{n}_L+1}\right]\left[\frac{\omega_T^s}{\omega_L^s}\right]^4\left[\frac{\omega_L}{\omega_T}\right]\left[\frac{\rho_{\text{expt}}}{\rho_{\text{theor}}}\right]\right]^{1/2}\right\}^{-1}. \tag{4}$$

where $\bar{n}_{T(L)}$ and $\omega_{T(L)}^s$ are the statistical factors and the absolute frequencies of the Stokes-scattered light, respectively, for T (L) phonons, ρ_{expt} is the observed ratio P_L/P_T of the integrated scattered powers, and ρ_{theor} a correction factor specific of the experimental configuration used for obtaining P_T and P_L.[27] In order to obtain ρ_{expt} a spectrum with $X=0$ was recorded in the configuration 90°(**a**)VH which yields both TO and LO scattering with $\rho_{\text{theor}}=1$ (Table I of Ref. 8). All slits of the spectrometer were wide open to assure that the areas under the triangular peaks observed represent accurately the powers, P_T and P_L. The measured ratio is $\rho_{\text{expt}}=2.1\pm0.1$ which, with the usual choice of the minus sign in Eq. (4), yields for InP at 300 K and $\lambda=1.06$ μm, $C=-0.52\pm0.03$. This value agrees very well with other experimental results (-0.53, Ref. 28). Theoretical estimates[29,30] are lower in magnitude, that of Ref. 30 (-0.40) being fairly close to the one reported here.

B. FIR reflectivity measurements

All the faces of the samples (n type, 2×10^{15} cm^{-3}) were polished and etched in methanol with 0.05% Br_2 for 5 min. The etching procedure turned out to be critical for the shape of the reststrahlen band. Any residual surface damage produced during the polishing, and not removed by etching, caused lowering of the reflectivity plateau which, in turn, affected the results of the fit with a harmonic oscillator. Only the **b** and **c** crystal orientations were found to be necessary. The maximum stresses reached were 0.6 and 1.0 GPa, respectively. The light was polarized either parallel ($\parallel$) or perpendicular ($\perp$) to the stress axis, leading to information about the singlet or doublet phonon components, respectively.

The reflectivity spectra were fitted to a harmonic oscillator model without a Drude term since no plasma edge was observed (low free-carrier concentration). The phonon frequencies ω_σ and a single damping constant Γ were used as free parameters. Optical and photoelastic constants were taken as fixed parameters (Table III). Otherwise the same fitting algorithm was used as in Ref. 5. An example of spectra and fitting curves is shown in Fig. 4. The dependence of $\Delta\Omega$ on stress obtained with this procedure is shown in Fig. 5. The slopes derived from a linear least-squares fit are included in Table I. The average Grüneisen parameters and the PDP's calculated from these slopes are listed in Table II for comparison with those from the IRRS experiments. The former values are systematically lower due to stress relaxation near the surface, as will be discussed in the following section. Since the PDP's obtained from the IRRS work are more representative of the bulk properties of the material, we regard these values as most appropriate for InP and use them for the calculation of all other parameters listed in Table III. The $X=0$ values of the phonon frequencies derived from the fits are $\omega_{T(L)}=303.7$ (345.0) cm^{-1}, i.e., the same as those of Ref. 20.

Contrary to the IRRS experiments where the material is transparent to the probing ir laser radiation, in the FIR experiments the ir radiation probes only a layer of the material at the surface. The thickness of the layer is determined by the penetration depth d of the ir radiation. This depth varies rather drastically with the frequency ω in the region of the reststrahlen band; this has to be taken into consideration when comparing results of the three types of experiments. The penetration depth d is related to the real (ϵ_1) and imaginary (ϵ_2) part of the dielectric function, as

$$\frac{1}{d}=\frac{4\pi\omega}{\sqrt{2}}[-\epsilon_1+(\epsilon_1^2+\epsilon_2^2)^{1/2}]^{1/2}, \tag{5}$$

with ω in cm^{-1}. Thus d can be obtained from the harmonic oscillator model for $\epsilon(\omega)$ (no Drude term included):

$$\epsilon(\omega)=\epsilon_\infty\left[1+\frac{\omega_L^2-\omega_T^2}{\omega_T^2-\omega^2-i\omega\Gamma}\right], \tag{6}$$

TABLE III. Numerical values of physical constants of InP and results of calculations of parameters relevant to the present work. For definitions, see text.

S_{11}	1.64
S_{12} (10^{-2}/GPa)[a]	-0.59
S_{44}	2.17
$\omega_{T(L)}$ (cm^{-1})[b]	303.7(350.6)±0.05
$\epsilon_\infty(\epsilon_0)$[a]	9.61(12.61)
$k_{11}^e(k_{11}^o)$	11.1±3.9[c] (26.2±5.5)[d]
$k_{12}^e(k_{12}^o)$	7.4±3.1 (14.9±4.5)
$k_{44}^e(k_{44}^o)$	6.9±0.9 (12.7±1.3)
$\tilde{M}_{11}$	1.8±0.3;[b,d] 1.3[e]
$\tilde{M}_{12}$	0.2±0.3; 0.1[e]
$\tilde{M}_{44}$	0.7±0.1; 0.7[e]
γ^*	-0.7 ± 0.2,[b,d] -0.6,[f] -0.44[e]
$\frac{\partial\ln\epsilon_\infty}{\partial\ln V}$ $[e_T^*(e)]$	0.9±0.3, [2.54,[f]2.35[e]]
$\frac{\partial e_T^*}{\partial P}$ ($10^{-2}e$/GPa)	-2.4,[b,d,f] -2.1[b,d,e]
C	-0.52 ± 0.03,[b] -0.53,[g] -0.46 ± 0.03[h] -0.14,[i] -0.40[j]

[a]Reference 17.
[b]Present, IRRS.
[c]References 22–24.
[d]Reference 21.
[e]Reference 25.
[f]Reference 20.
[g]Reference 28.
[h]Present, VISRS.
[i]Theory, Ref. 29.
[j]Theory, Ref. 30.

where values obtained from the harmonic oscillator fit to the reflectivity spectra should be used for $\omega_{T,L}$ and Γ. Figure 6 represents the dispersion of $d(\omega)$ in the region of interest, based on the $R(\omega, X=0)$ spectrum of Fig. 4(a).

According to Fig. 6, the penetration depths d_T and d_L at ω_T and ω_L are 0.2 and 20 μm, respectively. This means that the data at ω_T are more sensitive to surface conditions (e.g., strain relaxation) than at ω_L, the measured values of the latter possibly approaching the bulk values. This point will be further discussed in the last section.

C. Raman scattering in the visible

The same sample characteristics and preparation details apply as in Sec. III B. We used **a**, **b**, and **c** crystal orientations in the nearly backward scattering configuration with incidence at $\sim 55°$ and detection along the normal. The incident-scattered light polarizations were *HV*, (*HH*, *HV*), and (*VV*, *HV*, *HH*) in **a**, **b**, and **c**, respectively, leading to the components *Ld*, (*Ts*, *Td*), and (*Ts*, *Td*, *Ld*), respectively. No information about the *Ls* components can be obtained from backward configurations.

As in other piezo-Raman experiments with opaque materials[2,3,12,31] the present measurements suffer from large uncertainties in determining small frequency shifts due to poor signal-to-noise ratios. Accidental local heating of the scattering volume by the laser beam often posed additional difficulties because of the tendency of the phonon frequencies to soften with increasing temperature (for InP, $d\omega/dT \approx -0.02$ cm^{-1}/K, Ref. 32). In spite of these problems plots like those of Fig. 5 became possible. The slopes for the phonon components given above were determined through a linear least-squares fit and are in units of cm^{-1}/GPa, *Ld*: -2.0 ± 0.7, (*Ts*: -0.2 ± 0.4; *Td*: -1.4 ± 0.6), and (*Ts*: -1.7 ± 0.7; *Td*: -0.5 ± 0.8; *Ld*: -0.9 ± 0.6) in the **a**, **b**, and **c** configurations, respectively. The large error bars reflect the difficulties described above. Nevertheless it is clear that the slopes are systematically lower than their counterparts from the FIR experiments (see Table I).

As we will discuss in the following section, this is probably due to the small penetration depth d_{vis} of the laser radiation relative to d_T and d_L of Fig. 6. Indeed, with $\lambda=476.5$ nm, $\epsilon_1=14.9$, and $\epsilon_2=4.5$ (Ref. 33) we find, from Eq. (5), $d_{vis}=650$ Å $< d_T$ and d_L, which means that

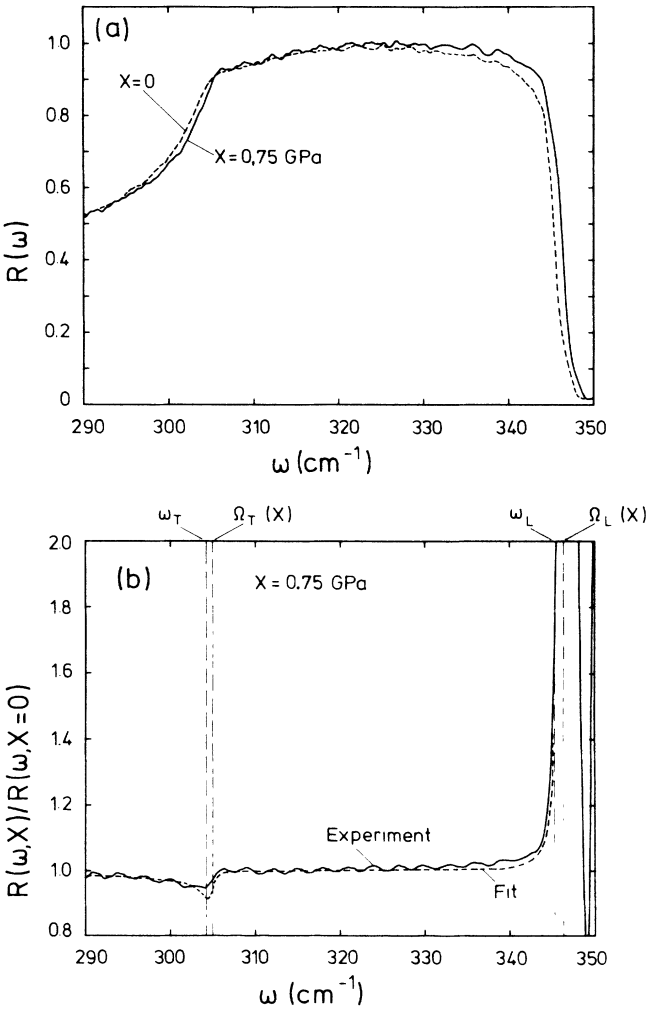

FIG. 4. (a) FIR reflectivity spectra of InP at 300 K with $X=0$ and 0.75 GPa along [111], and light polarization perpendicular to X. (b) Experimental and fitting curves for the ratio $R(X)/R(0)$ based on (a). The phonon frequencies $\omega_{T,L}$ and $\Omega_{T,L}(X)$ are shown by dashed lines.

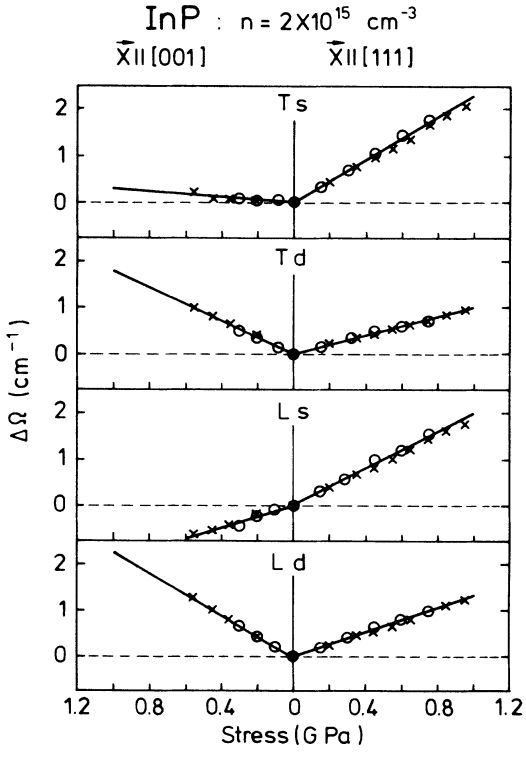

FIG. 5. Stress dependence of the phonon frequency shifts based on FIR reflectivity spectra like those in Fig. 4. The uncertainties are ±0.025 cm^{-1}. The straight lines represent linear least-squares fits for the joint data of two identical samples ($\times$ and $\circ$). Their slopes are included in Table I under the designation $\parallel$ and $\perp$.

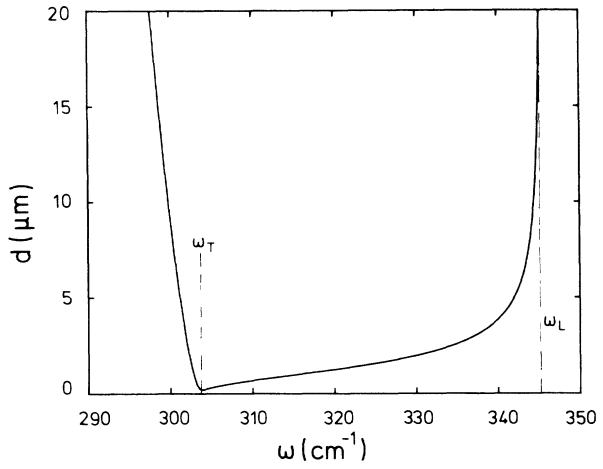

FIG. 6. Calculated penetration depth vs ir radiation frequency in the region of reststrahlen band for undoped InP. Dashed-dotted lines indicate the TO- and LO-phonon frequencies.

the slopes obtained in the VISRS work are even more surface sensitive than those from the FIR experiments.

In view of the large errors in the above slopes we did not use them for calculation of the relevant PDP's. However, we did calculate the Faust-Henry coefficient $C_{\rm vis}$ using P_T and P_L obtained through VISRS. The 180°(c)*HH* geometry which yields both TO and LO spectra was used. After instrumental correction we found $\rho_{\rm expt}=3.5\pm0.2$. For exact backward scattering the ratio $\rho_{\rm theor}$ would be 2. However, here we have used incidence at 55° and this reduces $\rho_{\rm theor}$ to 1.58 (Ref. 27). With this information we find from Eq. (4) that $C_{\rm vis}=-0.46\pm0.03$, which is marginally larger than the value at 1.06 μm (i.e., -0.52 ± 0.03). Because of the large error bars it is not clear whether a genuine difference, arising from resonance effects (frequency dependence of C), exists. Note that, above the absorption edge, C actually becomes complex and the ratio of LO to TO intensities is not sufficient to extract its real and imaginary parts. The theoretical calculations of $C(\omega)$ in Ref. 30 do not extend to 476.5 nm; hence no comparison with the present experiments can be made.

IV. DISCUSSION

The main objective of this work is to establish accurate values for the phonon deformation potentials and the strain coefficients of the effective charge of InP. Three independent spectroscopic procedures were followed. The first, IRRS, led to a complete set of values for such parameters which are representative of the bulk properties of the material. We list them in Tables II and III as the suggested values. The second, FIR reflectivity, also led to complete and accurate values for the same parameters which are more representative of regions near the surface of the material. The same situation occurs in the third type of experiments, VISRS, where again the information obtained should be even more surface sensitive and, in addition, the numerical values suffer from large experimental errors. The IRRS values suggested as being the most accurate ones have the same sign and order of magnitude as those reported for GaAs (Ref. 6) and AlSb,[8] the only other III-V semiconductors which have been investigated with the IRRS technique.

It is interesting that even at the highest stresses attained there were no signs of plastic deformation in our measurements (i.e., permanent deformation of spectra after removing the stress). It is known[34] that InP fractures as a brittle material at temperatures below $0.55T_m$ ($T_m=1335$ K being the melting point). This is exactly how our samples behaved once their breaking point was reached. On the other hand, we have no definite explanation for the weak nonlinearities observed in the curves of Figs. 2 and 3 (quadratic coefficient B of Table I). The fact that the same experimental setup and procedure was used for GaAs and AlSb with no traces of measurable nonlinearities makes us suspect that they may indeed be a property of the material. Thus, we have used for the determination of PDP's the slopes A obtained from the quadratic fits instead of those (a) from the linear fits. We note, however, that the dependence of phonon frequencies on hydrostatic pressure reported in Ref. 20 is considerably more linear than the dependence on uniaxial pressure reported here.

The relaxation of stress near the surface, on the other hand, as manifested by the decreasing slopes in the sequence of the three types of experiments in Secs. III A–III C, has already been observed in GaAs.[6,5,31] Having established the dispersion $d(\omega)$ of Fig. 6, we undertook an exploratory model calculation of the reflectivity spectrum in the presence of a linearly varying stress in the surface region. We have assumed that the stress decreases from its bulk value, at distance D from the surface, to half that value at the surface. This seems to be a reasonable speculation based on the numerical results of the Grüneisen parameters obtained from the three experiments. The region D was divided into 100 equal layers each having constant optical properties. The latter were calculated from the average stress value at the position of the layer. The stress determines the corresponding TO and LO frequencies in the layers and from Eq. (6) a dielectric function can be assigned to each layer. The spectrum of the total reflectivity was then calculated with a multilayer scheme from classical optics.[35] The stress relaxation parameter D was varied from 0.1 to 100 μm. The following three types of results were confirmed.

(a) For $D>d_L,d_T$, the reflectivity spectrum leads to smaller slopes $\Delta\Omega/X$ than the ones observed in the IRRS experiments.

(b) For $D<d_T,d_L$, the slopes are the same as in the IRRS experiments.

(c) For $d_T\le D\le d_L$, the slope for the TO (LO) phonon is smaller than (nearly equal to) that in the IRRS experiment.

Since the experimental results concur with case (a), we can only conclude from this discussion that $D>d_L$ where from Fig. 6, $d_L=20$ μm. It was also established from

these calculations that for compressive stresses and with $D \geq d_L$ given, the LO edge of the reststrahlen band is not affected except for a parallel shift.

A reasonable extension of the present work would be the study of doped InP with FIR reflectivity and IRRS techniques. Such measurements would lead to information on the effects of stress on the free-carrier parameters.[5] As for other choices of materials for which precise values of PDP's are highly desirable, we can mention AlAs, the importance of which in strained superlattices cannot be overemphasized. Unfortunately, AlAs is not available in bulk single crystals. Different sample configurations (films on substrates) in the presence of biaxial rather than uniaxial stresses may lead to acceptable results. The direct energy gap at $E_g = 2.9$ eV makes the IRRS approach usable.

Finally, silicon itself appears to be a good candidate in this regard. Its PDP's obtained from VISRS experiments[3] have been known, confirmed, and used for a long time, but a repetition of such experiments with a Nd:YAG laser may be of interest. Although the direct gap lies at 3.3 eV, the indirect gap at 1.18 eV makes Si rather opaque to visible lasers. Such measurements, however, might only become possible at low temperatures (the indirect gap is well above the laser frequency) since at room temperature the indirect gap luminescence will most certainly overcome the Raman spectrum.

ACKNOWLEDGMENTS

We would like to thank E. Kisela (deceased) and his co-workers at the Max-Planck-Institut (MPI) and C. Ostlender at Rheinisch-Westfälischen Technischen Hochschule (RWTH) Aachen for expert crystal preparation. One of us (E.A.) thanks H. Hirt, M. Siemers, and P. Wurster for technical assistance during the ir Raman measurements at the MPI. Thanks are also due to G. Müller of the "Universität Erlangen–Nürnberg" for supplying InP crystals. The work performed in Aachen and Athens was partially supported by the German and Greek Ministries on Research and Technology, respectively.

[1]E. Anastassakis, in *Physical Problems in Microelectronics,* edited by J. Kassabov (World Scientific, Singapore, 1985), p. 128, and references therein.

[2]E. Anastassakis, in *Dynamical Properties of Solids,* edited by G. K. Horton and A. A. Maradudin (North-Holland, Amsterdam, 1980), Vol. 4, p. 157, and references therein.

[3]E. Anastassakis, A. Pinczuk, E. Burstein, F. H. Pollak, and M. Cardona, Solid State Commun. **8**, 133 (1970).

[4]B. A. Weinstein and M. Cardona, Phys. Rev. B **5**, 3120 (1972).

[5]M. Hünermann, W. Richter, J. Saalmüller, and E. Anastassakis, Phys. Rev. B **34**, 5381 (1986).

[6]P. Wickboldt, E. Anastassakis, R. Sauer, and M. Cardona, Phys. Rev. B **35**, 1362 (1987).

[7]E. Anastassakis and M. Cardona, Solid State Commun. **64**, 543 (1987).

[8]E. Anastassakis and M. Cardona, Solid State Commun. **63**, 893 (1987).

[9]M. H. Grimsditch, E. Anastassakis, and M. Cardona, Phys. Rev. B **18**, 901 (1978).

[10]S. Venugopalan and A. K. Ramdas, Phys. Rev. B **8**, 717 (1973).

[11]A. D. Papadopoulos, Y. S. Raptis, and E. Anastassakis, Solid State Commun. **58**, 645 (1985).

[12]F. Cerdeira, C. J. Buchenauer, F. H. Pollak, and M. Cardona, Phys. Rev. B **5**, 580 (1972).

[13]I. Balslev, Phys. Status Solidi B **61**, 207 (1974).

[14]K. J. Bachmann, Annu. Rev. Mater. Sci. **11**, 441 (1981).

[15]D. Olego, T. Y. Chang, E. Silberg, E. A. Caridi, and A Pinczuk, Appl. Phys. Lett. **41**, 476 (1982), and references therein.

[16]H. Shen and F. H. Pollak, Appl. Phys. Lett. **45**, 692 (1984).

[17]*Landolt-Börnstein, Numerical Data and Functional Relationships in Science and Technology,* Vol. 17a, edited by O. Madelung, M. Schulz, and H. Weiss (Springer, New York, 1982), p. 281.

[18]M. Cardona, in *Light Scattering in Solids,* edited by M. Cardona and G. Güntherodt (Springer, Berlin, 1982), Vol. II, p. 61.

[19]The notation p, q, r (p', q', r') is often used in the literature for PDP's. In terms of the PDP's used here, these correspond to $K_{ij}^T = \omega_T^2 \tilde{K}_{ij}^T$ ($K_{ij}^L = \omega_L^2 \tilde{K}_{ij}^L$), for $ij = 11$, 12, and 44, respectively.

[20]R. Trommer, H. Müller, M. Cardona, and P. Vogl, Phys. Rev. B **21**, 4869 (1980).

[21]E. Anastassakis, J. Phys. C **16**, 3329 (1983).

[22]N. Suzuki and K. Tada, Jpn. J. Appl. Phys. **22**, 441 (1983).

[23]F. Canal, M. Grimsditch, and M. Cardona, Solid State Commun. **29**, 523 (1979).

[24]M. Hünermann, Diploma work, Technical University of Aachen, 1985 (unpublished).

[25]E. Anastassakis and M. Cardona, Phys. Status Solidi B **129**, 101 (1985).

[26]W. A. Harrison, *Electronic Structure and the Properties of Solids* (Freeman, San Francisco, 1980), p. 114.

[27]A. Anastassiadou, Y. S. Raptis, and E. Anastassakis, J. Appl. Phys. **60**, 2924 (1986), and references therein.

[28]N. Suzuki and K. Tada, Jpn. J. Appl. Phys. **23**, 291 (1984).

[29]C. Flytzanis, Phys. Rev. B **6**, 1264 (1972).

[30]A. Hernández-Cabrera, C. Tejedor, and F. Meseguer, J. Appl. Phys. **58**, 4666 (1985).

[31]A. K. Sood, E. Anastassakis, and M. Cardona, Phys. Status Solidi B **129**, 505 (1985).

[32]E. Liarokapis and E. Anastassakis (unpublished).

[33]D. E. Aspnes and A. A. Studna, Phys. Rev. B **27**, 985 (1983).

[34]G. T. Brown, B. Cockayne, and W. R. Maceman, J. Mater. Sci. **15**, 1469 (1980).

[35]B. Harbecke, Appl. Phys. B **39**, 165 (1986).